Improving surface rainfall mapping in complex terrain regions through lowering the minimum scan elevation angle of operational weather radar

Liangwei Wang, Haonan Chen, Robert Cifelli, Zhe Li

***Abstract*—The National Weather Service has initiated an effort to upgrade the scan strategy of the operational Weather Surveillance Radar – 1988 Doppler (WSR-88D) to improve its hydrometeorological applications. The lowest scan elevation angle has been changed from 0.5° to 0° (or even lower in future) for some WSR-88D stations. Using the KMUX WSR-88D radar deployed in mountainous terrain in Northern California as an example, this article quantifies the impacts of lowering the minimum scan elevation angle of WSR-88D radar on surface rainfall mapping, with an emphasis on shallow orographic precipitation. In order to estimate surface rainfall using radar observations, polarimetric radar rainfall relations are established using local disdrometer data, which are then implemented with the KMUX radar observations at 0° and 0.5° scan elevation angles to derive rainfall estimates. Comparative evaluation of the radar-based rainfall estimates using rainfall measurements from surface rain gauges has demonstrated the superior performance of the lower scan elevation angle. When the distance from the radar is long (i.e., when the radar beam is likely within or above the melting layer), the improvement gained by the 0° scan relative to the 0.5° scan is 16.1% and 19.5% in terms of the normalized standard error (NSE) and the Pearson correlation coefficient ($CORR$), respectively.**

***Index Terms*—Dual-polarization, Weather radar, orographic precipitation, WSR-88D, quantitative precipitation estimation**

I. Introduction

THE operational Weather Surveillance Radar–1988 Doppler (WSR-88D) network, or NEXRAD, plays a critical role in monitoring hydrometeorological conditions in the United States, serving as the cornerstone of national severe weather warning and forecast infrastructure [1]. However, the current regulations limit the lowest scan elevation angle of the operational WSR-88D to 0.5°, one-half the antenna beamwidth. Compounding the Earth's curvature, the WSR-88D network has severe limitations in observing the low part of the troposphere, where many hazardous weather events occur [2] [3] [4].

To improve hydrometeorology applications of WSR-88D such as surface rainfall mapping, the National Weather Service (NWS) has initiated an effort to upgrade the scan strategy of WSR-88D by adding lower scan elevation angles (0° or even lower in future). The KMUX radar, deployed on top of Mt Umanhum in the Santa Cruz Mountains in northern CA, is one of the first WSR-88D stations that executed a 0° scan elevation angle (since late 2018).

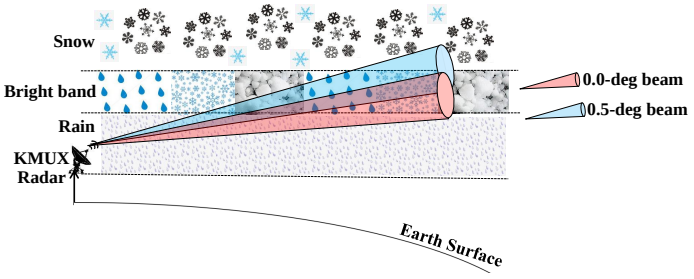

Fig. 1. Diagram illustrating the sampling limitations of KMUX WSR-88D in Northern California.

Typically, the orographic precipitation system in Northern California has a melting layer 1-1.5 km above sea level (ASL) [5]. Since the KMUX radar is deployed at an altitude about 1 km ASL, the 0.5° beam often observes the mixed-phase hydrometeors in the bright band or snowflakes above the bright band, even if it is raining on the ground (see Fig. 1 for illustration). This paper uses the KMUX radar as an example to quantify the improvements brought by the enhanced WSR-88D scan strategy. Specifically, we derive and compare the surface rainfall estimates based on the KMUX radar observations at both 0.5° and 0° scan elevation angles. For radar-based rainfall estimation, we derive polarimetric radar rainfall relations using local raindrop size distribution (DSD) data, and then apply the derived relations to both 0.5° and 0° scan elevation angles. The results of different radar scan elevation angles are investigated at different distances from the radar to quantify the added-value of the 0° scan for surface rainfall mapping.

The remainder of this article is organized as follows. Section II describes the study domain and selected precipitation events used in this article. Polarimetric radar rainfall estimation algorithms and results are detailed in Section III. A discussion about the radar rainfall estimation performance is also provided in Section III. Concluding remarks are provided in Section IV.

II. Study Domain and Selected Precipitation Events

The study domain is centered around the KMUX radar in the San Francisco Bay Area, CA, which supports one of the

This research was supported by the National Oceanic and Atmospheric Administration (NOAA) through Grant NA19OAR4320073. *(Corresponding author: Haonan Chen.)*

Liangwei Wang, Haonan Chen, and Zhe Li are with the Department of Electrical and Computer Engineering, Colorado State University, Fort Collins, CO 80523, USA (e-mail: haonan.chen@colostate.edu).

Robert Cifelli is with the NOAA Physical Sciences Laboratory, Boulder, CO 80305, USA.

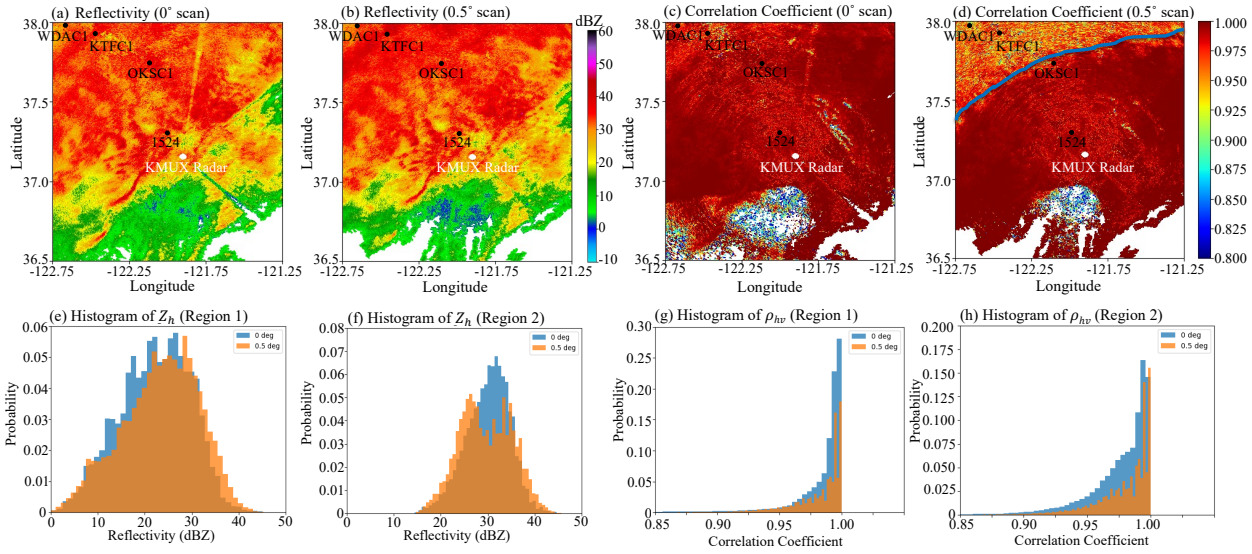

Fig. 2. KMUX radar observations at 0215UTC, October 25, 2021: reflectivity Z_h of (a) 0° scan and (b) 0.5° scan; correlation coefficient ρ_{hv} of (c) 0° scan and (d) 0.5° scan. Histogram of KMUX radar observations over two subdomains (Region 1 is within 70 km from the KMUX radar, and Region 2 is 70-100 km from the KMUX radar): reflectivity Z_h in (e) Region 1 and (f) Region 2; correlation coefficient ρ_{hv} in (g) Region 1 and (h) Region 2. The black dots in (a)-(d) represent four ground surface rain gauge stations used as references

most prosperous economies in the United States. Due to the unique geography and their exposure to atmospheric rivers (AR), there are many flood-prone regions in this area [5] [6] [7]. Hence, accurate rainfall mapping is critical to balancing the competing needs of water supply and flood mitigation [4].

In this article, we select two typical precipitation events, namely, 27-28 January 2021 and 24-25 October 2021, to quantify the hydrometeorological impacts of lowering the minimum scan elevation angle of KMUX radar. The two events occurred after November 2018, when the 0° scan was implemented by the KMUX radar. Both events are associated with AR, thus can represent the local heavy precipitation characteristics to a large extent [5] [8]. Polarimetric radar observations from the KMUX radar at both 0.5° (the minimum scan angle before November 2018) and 0° scan elevation angles during these two precipitation events are investigated and are used to derive rainfall estimates. The rainfall estimates are comparatively evaluated using surface rain gauge measurements at different distances from the KMUX radar (see Fig. 2). Nevertheless, it should be noted that the goal is not to produce optimal rainfall estimates for this study domain. Rather, we would like to highlight the improvement brought by the lower scan elevation angle, especially at longer distances.

III. Methodology and Results

A. Methodology

In this study, the polarimetric radar observations, including reflectivity Z_h, differential reflectivity Z_{dr}, specific differential phase K_{dp}, and correlation coefficient ρ_{hv}, from the two scan elevation angles are investigated and are used to produce surface rainfall estimates. For rainfall estimation, this article derives the locally adapted radar rainfall relations based on the DSD measurements collected during November 2018 through May 2019, from a disdrometer deployed in Santa Clara, CA. In particular, using the T-matrix scattering approach, the DSD data are utilized to simulate the polarimetric radar variables at S-band (i.e., WSR-88D operating frequency). The corresponding rainfall rates R are also calculated using the DSD data. Then, 70% of the data are used to obtain the DSD-fitted radar rainfall relations, i.e., $R(Z_h)$, $R(K_{dp})$, $R(Z_h, Z_{dr})$, and $R(K_{dp}, Z_{dr})$, based on nonlinear least squares regression.

To assess the effectiveness of the radar rainfall relations that were locally fitted, the normalized standard error (NSE, expressed as a percentage), Pearson correlation coefficient ($CORR$, dimensionless), and root mean square error ($RMSE$, measured in mm/hr) are calculated for these relations by utilizing the 30% independent testing DSD dataset.

$$CORR = \frac{\sum[(R_R - < R_R >)(R - < R >)]}{\sqrt{\sum(R_R - < R_R >)^2}\sqrt{\sum(R - < R >)^2}} \quad (1a)$$

$$NSE = \frac{< |R_R - R| >}{< R >} \quad (1b)$$

$$RMSE = \sqrt{< (R_R - R)^2 >} \quad (1c)$$

where R_R and R represent rainfall estimates from simulated radar parameters and the counterparts directly calculated from DSD data, respectively. The angle brackets stand for sample average.

The DSD-fitted radar rainfall relations are then applied to the KMUX radar observations at 0° and 0.5° scan elevation angles to produce surface rainfall estimates during the two precipitation events. To compare and evaluate the radar-derived rainfall estimates, a similar set of metrics to Eq. 1 is used. However, instead of using rain rates directly computed from DSD as references, rainfall measurements from four rain gauges (black dots in Fig. 2) are used as references in practical applications.

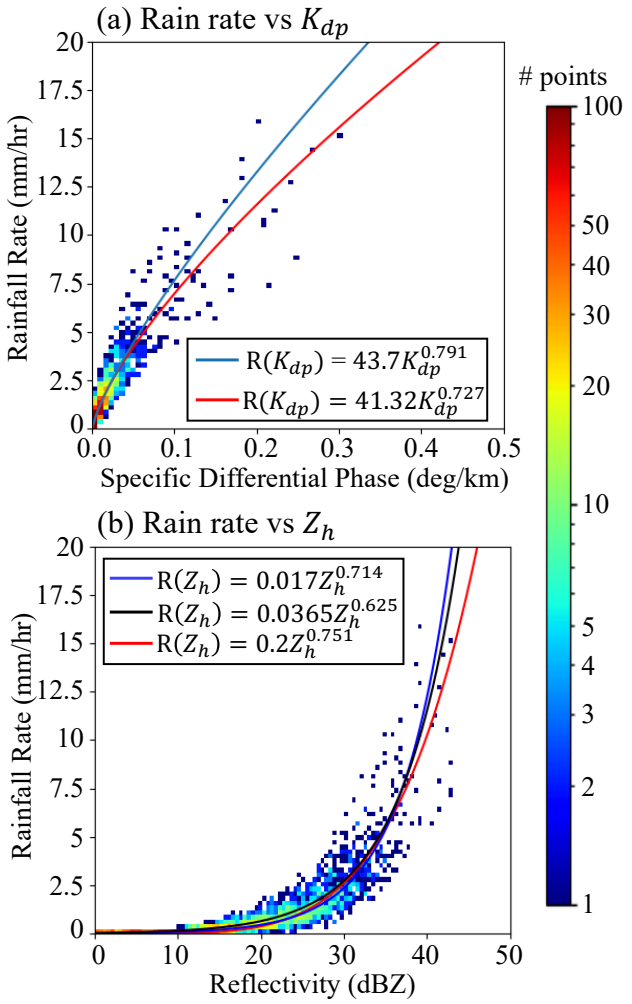

Fig. 3. (a) Scattergram of rainfall rate R versus K_{dp}. The red line indicates the locally fitted radar rainfall relation, whereas the blue line shows a selected $R(K_{dp})$ relation used for convective rainfall estimation [9] [10]. (b) Scattergram of rainfall rate R versus Z_h. The red line indicates the locally fitted relation, whereas the blue and black curves show the WSR-88D $Z-R$ relation [1] for convective rain and Marshall-Palmer $Z-R$ relation [11] for stratiform rain, respectively. Note that the color-coded rain rates and radar variables are all computed from disdrometer data in Northern California.

B. Results

As an example, Fig. 2 presents the KMUX radar reflectivity and correlation coefficient from two elevation angles at 0215UTC, 25 October 2021. Comparison between 0° and 0.5° data indicates that there is a regional boundary around 70 kilometers (as outlined by the blue line in Fig. 2(d)) from the radar station, beyond which the correlation coefficient from the 0.5° scan is noticebly lower, suggesting that the 0.5° beam was observing within or above the melting layer.

To gain more insights into the observation difference, we further separate the radar coverage domain into two subregions depending on the distance from the radar site. Region 1 is within 70 km from the radar, whereas Region 2 is 70-100 km from the radar. Figs. 2 (e)-(h) show the histograms of KMUX radar reflectivity and correlation coefficient for the two subregions, which highlight that the reflectivity is narrower and there is a higher concentration of correlation coefficient closer to 1 for the 0° scan, especially over Region 2. In addition, both the narrower reflectivity and the more prevalent correlation coefficient close to 1 is consistent with the 0° scan sampling in the liquid region of the storm compared to the 0.5° scan. The higher liquid concentration of 0° scan observations indicates positive impacts of lowering WSR-88D scan elevation angle on surface rainfall estimation, which will be demonstrated in this section.

Based on the DSD data, the locally-fitted radar rainfall relations are obtained as follows:

$$R(K_{dp}) = 41.32K_{dp}^{0.727} \tag{2a}$$

$$R(Z_h) = 0.02Z_h^{0.751} \tag{2b}$$

$$R(Z_h, Z_{dr}) = 0.0118Z_h^{0.881}Z_{drl}^{-4.103} \tag{2c}$$

$$R(K_{dp}, Z_{dr}) = 103.9K_{dp}^{0.891}Z_{drl}^{-2.235} \tag{2d}$$

Here, Z_h (mm^{6}m^{-3}) is the reflectivity factor at horizontal polarization and $Z_{drl} = 10^{Z_{dr}/10}$ is differential reflectivity in linear scale.

For illustration purposes, Fig. 3 shows the scattergrams of the DSD-derived rainfall rates versus K_{dp} and reflectivity (Z_h; in dBZ). The locally fitted relation (in red) and other commonly used radar rainfall relations are also indicated in Fig. 3. Overall, it can be seen that the locally fitted relations demonstrate a better performance in fitting the DSD-based observations, especially at high rain rate values ($>$ 5 mm/hr). Nevertheless, since this study domain is often characterized by shallow stratiform rain with low rain rates, we expect that the difference between different radar rainfall relations may not be significant in practical applications.

To quantify the parameterization errors of the radar rainfall relations in Eqs. 2, $CORR$, NSE, and $RMSE$ scores are computed for these relations based on the testing DSD data, and the results are summarized in Table I. According to these statistics, the $R(K_{dp}, Z_{dr})$ relation shows the best performance, with the highest $CORR$ and the lowest $RMSE$ values. Therefore, this new radar rainfall relation (Eq. 2d) is applied to the KMUX radar observations from 0° and 0.5° scans to quantify the benefit brought by lowering the minimum scan elevation angle for surface rainfall estimation. After obtaining rainfall estimates using the $R(K_{dp}, Z_{dr})$ relation based on the 0° and 0.5° scan data during the two selected precipitation events, rainfall measurements from four rain gauges are used as references to quantify the radar QPE performance. Two rain gauges are located in each subregion (OKSC1 and 1524 in Region 1; WDAC1 and KTFC1 in Region 2); selection of these gauges can be used to help us quantify both the QPE impact of lowering the KMUX radar scan elevation angle and the assessment of QPE performance at different ranges from the KMUX radar.

Figure 4 illustrates the accumulated rainfall at two validation gauge locations of two precipitation events from 0000UTC, October 24 to 0000UTC, October 26, 2021, and from 0000UTC, January 27 to 0000UTC, January 29, 2021, including rainfall estimates from the KMUX radar observations at 0° and 0.5° scan elevation angles, as well as rainfall measurements from the gauges. Here, we meant to show the estimates from one gauge in Region 1 (OKSC1) and one in

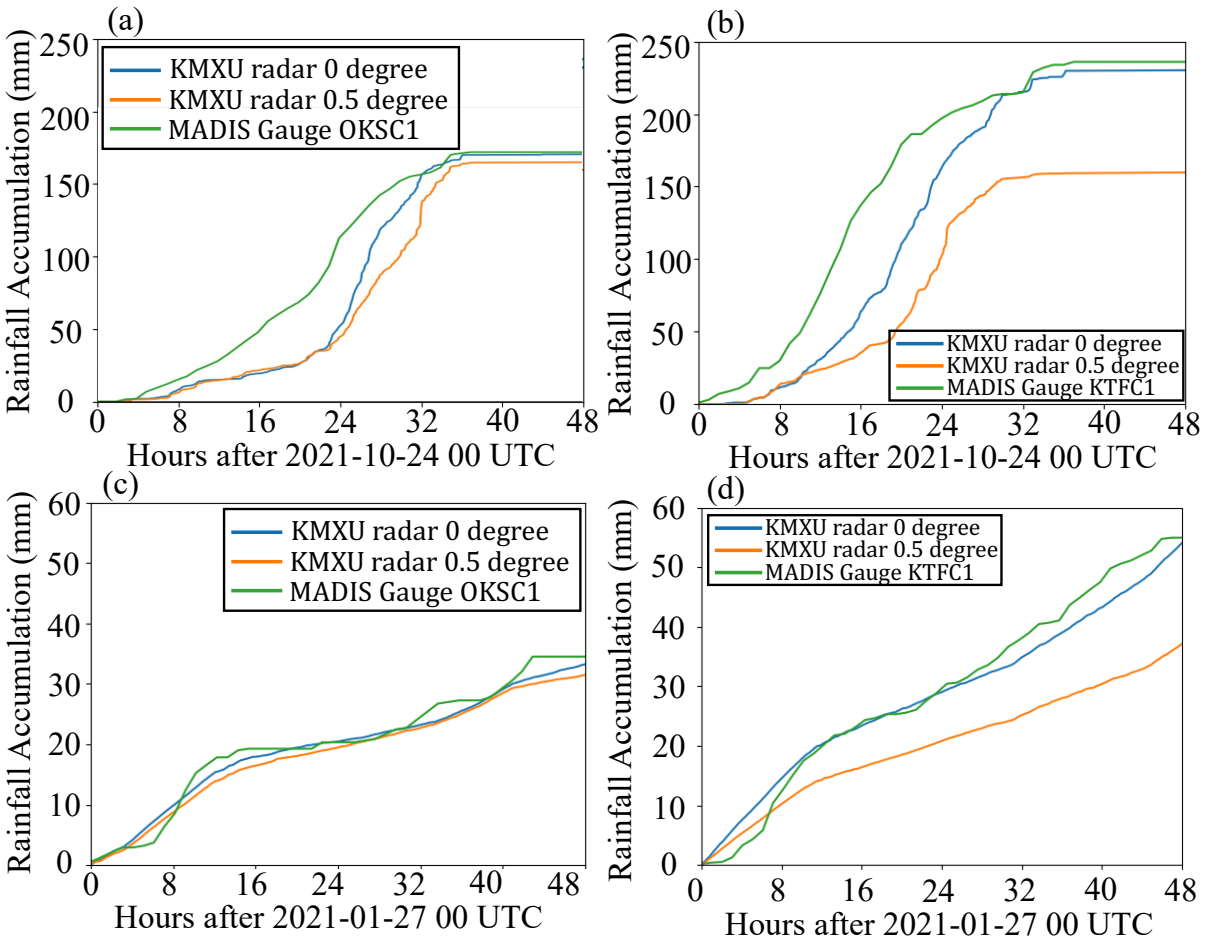

Fig. 4. Comparison of rainfall accumulations of two precipitation events: (a-b) from 0000UTC, October 24 to 0000UTC, October 26, 2021; (c-d) from 0000UTC, January 27 to 0000UTC, January 29, 2021. Both radar rainfall estimates derived from 0° and 0.5° elevation angles of KMUX radar, and the corresponding surface rainfall measurements at two gauge locations are illustrated.

TABLE I
EVALUATION RESULTS OF THE PARAMETERIZATION ERRORS OF DIFFERENT RADAR RAINFALL RELATIONS BASED ON THE INDEPENDENT DSD DATA: NSE, $CORR$, AND $RMSE$.

Radar rainfall relation	NSE	$CORR$	$RMSE$
$R\left(K_{dp}\right) = 41.32K_{dp}^{0.727}$	25.17%	0.969	0.383
$R\left(Z_h\right) = 0.02Z_h^{0.751}$	26.28%	0.936	1.217
$R\left(Z_h, Z_{dr}\right) = 0.0118Z_h^{0.881}Z_{drl}^{-4.103}$	33.09%	0.965	0.436
$R\left(K_{dp}, Z_{dr}\right) = 103.9K_{dp}^{0.891}Z_{drl}^{-2.235}$	18.88%	0.985	0.279

Region 2 (KTFC1) to highlight the relative performance of rainfall estimates at different distances from the radar. The performance at other gauge locations which are not shown in Fig. 4 is similar.

In general, radar rainfall estimates from the 0° scan have the most pronounced performance than those from the 0.5° scan, and the difference is large at long distances (see Fig. 4b), consistent with the 0° beam remaining in the liquid region below the melting layer over a larger portion of the domain compared to the 0.5° beam (see Fig. 1). For a more comprehensive verification, Fig. 5 shows the quantitative evaluation results of hourly QPE derived from 0° and 0.5° scan data during the two selected precipitation events, based on rainfall measurements from all the four surface gauge stations. Fig. 5 clearly shows that the errors in radar rainfall estimates are reduced compared to 0.5° data using the 0° scan data, especially at long ranges from the radar (i.e., at gauge location WDAC1 and KTFC1 in Region 2). This is consistent with the radar data distributions in Fig. 2 and result comparisons in Fig. 4.

IV. SUMMARY AND CONCLUSION

Using the KMUX radar deployed in the San Francisco Bay Area as an example, this study quantifies the QPE impacts of upgrading the scan strategy of WSR-88D by lowering the minimum scan elevation angle from 0.5° to 0°. New radar rainfall relations were derived using DSD observations from a local disdrometer, then the optimal relation is applied to the KMUX radar data at 0° and 0.5° scan elevation angles during two typical AR-induced precipitation events in Northern California. Major conclusions are summarized as follows:

(1) The intercomparison of DSD-fitted local radar rainfall relations indicates that the $R(K_{dp}, Z_{dr})$ relation performs

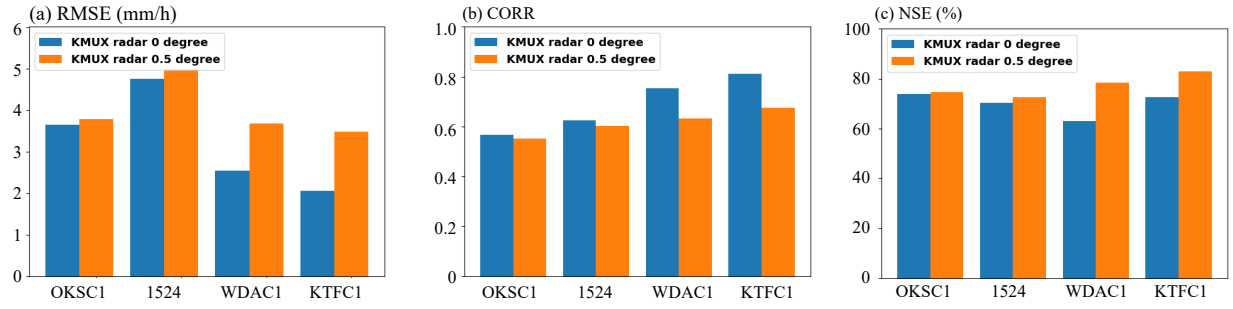

Fig. 5. Quantitative evaluation results of radar hourly QPE derived from 0° and 0.5° scan elevation angles during the two selected precipitation events: (a) $RMSE$ (mm/hr), (b) $CORR$ (unitless), and (c) NSE (%). These results are based on rainfall measurements from four validation gauges illustrated in Fig. 2.

the best with the highest $CORR$ and lowest $RMSE$ scores compared with the other three relations in this study area, i.e., $R(K_{dp})$, $R(Z_h)$, and $R(Z_h, Z_{dr})$.

(2) The radar QPE based on KMUX observations at different scan elevation angles are derived using the best locally fitted radar rainfall relation and the QPE products are evaluated using rainfall measurements from four surface rain gauges. It is found that radar QPE from 0° scan data is generally more accurate than that derived from 0.5° scan data.

(3) The relative improvement on radar QPE brought by lowering the KMUX WSR-88D radar scan elevation angle at different detection ranges is further assessed by grouping the gauges into two categories in terms of their distance from the radar site (within 70 km versus beyond 70 km). This conditional analysis highlights that the lower scan elevation angle (i.e., 0°) data has significantly improved the radar QPE performance at long distances from the radar, where the radar beams are likely intersecting or overshooting the melting layer.

However, it should be noted that radar QPE uncertainty is determined by many physiographic factors [7]. Incorporating the vertical structure of radar observations and topographical information in complex terrain [5] to further improve radar QPE performance should be investigated in future. In addition, similar demonstration study with WSR-88D stations at other geophysical regions and different seasons should be conducted to fully understand when and where the upgraded scan strategy can help with radar-based quantitative precipitation estimation.

Acknowledgments

The authors would like to acknowledge the Santa Clara Valley Water regarding the potential applications of the derived KMUX radar rainfall estimates. The KMUX radar data used in this study are available from the NOAA National Centers for Environmental Information at https://www.ncdc.noaa.gov/nexradinv/. We also thank the anonymous reviewers for providing careful reviews and comments on this article.

References

[1] R. A. Fulton, J. P. Breidenbach, D.-J. Seo, D. A. Miller, and T. O'Bannon, "The WSR-88D Rainfall Algorithm," *Weather and Forecasting*, vol. 13, no. 2, pp. 377 – 395, 1998.

[2] V. Chandrasekar, H. Chen, and B. Philips, "Principles of high-resolution radar network for hazard mitigation and disaster management in an urban environment," *Journal of the Meteorological Society of Japan. Ser. II*, vol. 96, pp. 119–139, 2018.

[3] R. Cifelli, V. Chandrasekar, H. Chen, and L. E. Johnson, "High resolution radar quantitative precipitation estimation in the san francisco bay area: Rainfall monitoring for the urban environment," *Journal of the Meteorological Society of Japan. Ser. II*, vol. 96A, pp. 141–155, 2018.

[4] R. Cifelli, V. Chandrasekar, L. Herdman, D. D. Turner, A. B. White, T. I. Alcott, M. Anderson, P. Barnard, S. K. Biswas, M. Boucher, J. Bytheway, H. Chen, H. Cutler, J. M. English, L. Erikson, F. Junyent, D. J. Gottas, J. Jasperse, L. E. Johnson, J. Krebs, J. van de Lindt, J. Kim, M. Leon, Y. Ma, M. Marquis, W. Moninger, G. Pratt, C. Radhakrishnan, M. Shields, J. Spaulding, B. Tehranirad, and R. Webb, "Advanced quantitative precipitation information: Improving monitoring and forecasts of precipitation, streamflow, and coastal flooding in the san francisco bay area," *Bulletin of the American Meteorological Society*, 2022.

[5] H. Chen, R. Cifelli, and A. White, "Improving Operational Radar Rainfall Estimates Using Profiler Observations Over Complex Terrain in Northern California," *IEEE Transactions on Geoscience and Remote Sensing*, vol. 58, no. 3, pp. 1821–1832, 2020.

[6] D. Willie, H. Chen, V. Chandrasekar, R. Cifelli, C. Campbell, D. Reynolds, S. Matrosov, and Y. Zhang, "Evaluation of multisensor quantitative precipitation estimation in Russian River Basin," *Journal of Hydrologic Engineering*, vol. 22, no. 5, p. E5016002, 2017.

[7] H. Chen, R. Cifelli, V. Chandrasekar, and Y. Ma, "A flexible bayesian approach to bias correction of radar-derived precipitation estimates over complex terrain: Model design and initial verification," *Journal of Hydrometeorology*, vol. 20, no. 12, pp. 2367 – 2382, 2019.

[8] F. M. Ralph, P. J. Neiman, G. A. Wick, S. I. Gutman, M. D. Dettinger, D. R. Cayan, and A. B. White, "Flooding on california's russian river: Role of atmospheric rivers," *Geophysical Research Letters*, vol. 33, no. 13, 2006.

[9] Y. Wang and V. Chandrasekar, "Quantitative precipitation estimation in the casa x-band dual-polarization radar network," *Journal of Atmospheric and Oceanic Technology*, vol. 27, no. 10, pp. 1665 – 1676, 2010.

[10] H. Chen and V. Chandrasekar, "The quantitative precipitation estimation system for Dallas–Fort Worth (DFW) urban remote sensing network," *Journal of Hydrology*, vol. 531, pp. 259–271, 2015.

[11] J. S. Marshall and W. M. K. Palmer, "The distribution of raindrops with size," *Journal of Atmospheric Sciences*, vol. 5, no. 4, pp. 165 – 166, 1948.